Sliding Window Integrator Approximations for Multichannel Autocorrelation UWB Receivers

Andreas Pedross* and Klaus Witrisal*
*Graz University of Technology, Austria; {andreas.pedross,witrisal}@tugraz.at

***Abstract*—Noncoherent UWB receivers promise low power consumption and low processing complexity but their peak data rate is limited by the delay spread of the multipath radio channel. A recently proposed multichannel autocorrelation receiver (AcR) can break this rate limit because it can demodulate multicarrier signals. The hardware implementation of this receiver architecture is addressed in this paper. We focus on the integration device, which is part of the AcR and essential to suppress nonlinear cross-products between data carriers. Passive filter structures are analyzed for this purpose. It is shown that the optimized filter outperforms the reference system using an ideal sliding window integrator because it is able to mitigate more system noise.**

I. Introduction

Noncoherent receivers are a possible way forward to exploit the advantages of UWB technology in low-complexity, low-power devices [1]. However, their simplicity comes at the cost of reduced robustness in presence of noise and multipath interference. For instance to achieve high data rate using an energy detection receiver, a rather hard limit is set by the excess delay of the multipath channel. Equalization schemes achieve limited gains only [2].

An alternative approach to increasing the data rate is multicarrier transmission [3], [4], where an analog frontend is used to separate the received signal into its subcarriers. The subcarriers can be sampled and processed at much lower bandwidth; typically at symbol rate. A fixed implementation of a suitable filter bank would result in a very robust high-rate receiver, but it would require highly selective frontend filters and lack any flexibility concerning the band selection. The flexibility improves with the receiver architecture described in [4], which performs an autocorrelation operation in the analog frontend (cf. Fig. 1) and leaves the bandselection to a digital backend running at moderately slow symbol rate.

This paper addresses the hardware requirements of the latter receiver. It concentrates on the integration and sampling blocks, which have an essential role in suppressing cross-products between subcarriers that arise in the nonlinear frontend. We investigate passive filter structures combined with conventional ADCs. This yields a solution that can potentially be realized using standard building blocks and it may save power compared with an active design as in [5].

The paper is organized as follows. In Section II a review of the multichannel AcR system is given for a better understanding of the integrator design constraints. The passive filter design is addressed in Section IV. The analysis and system performance concerning the signal, noise, and self-interference is given in Section V. In Section VI bit-error-rate comparisons are shown, followed by conclusions.

This work is conducted in the framework of the NOFDM project, a collaborative project funded by the Austrian Research Promotion Agency (FFG), grant number 825899.

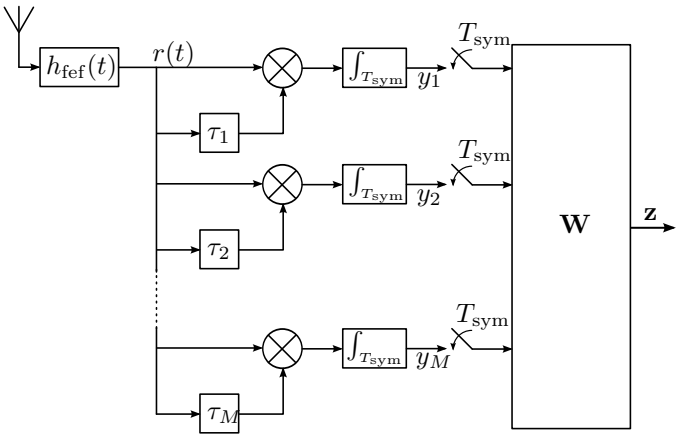

Fig. 1. The multichannel AcR architecture consists of delay filters, multiplication devices, and integration filters.

II. Review of the MC-AcR

The aim of the multichannel AcR is to avoid the need for directly sampling the passband signal, which would require sampling-rates of several GSamples/s. The crucial signal processing is the computation of a short-time estimate of the autocorrelation function for the delays $\{\tau_m\}$. It is done in the analog domain, therefore the received signal only needs to be sampled at symbol-rate R_{sym}.

The system is briefly reviewed below to understand the requirements of the sliding window integrator in the multichannel AcR system.

Assuming an inter-symbol-interference (ISI) free scenario, by introduction of a sufficient long zero guard interval, our analysis can concentrate on a single transmitted symbol with period T_{sym}. The transmitted signal can be written as

$$s(t) = \Re\left\{ e^{+j\omega_{\mathrm{c}}t} \sum_{k=-\frac{K-1}{2}}^{+\frac{K-1}{2}} s_k \varphi(t) e^{+jk\omega_{\mathrm{sc}}t} \right\}, \qquad (1)$$

where s_k is the $(\frac{K+1}{2}+k)$-th element of a K-dimensional symbol vector $\mathbf{s}$, $\varphi(t)$ is the sub-carrier pulse shape, ω_{sc} is the sub-carrier spacing, ω_{c} is the center frequency, j is the imaginary

unit, and $\Re\{.\}$ is the real operator. The terms $\varphi(t)\, e^{+jk\omega_{\rm sc}t}$, with $k \in \mathcal{K}$, $\mathcal{K} = \left\{-\frac{K-1}{2}, ..., +\frac{K-1}{2} \mid K \text{ is odd}\right\}$, are orthogonal basis functions which span a K-dimensional signal space.

The received signal is given as

$$r(t) = h_{\rm ch}(t) * s(t) + n(t) \tag{2}$$

$$= \Re\left\{ e^{+j\omega_{\rm c}t} \sum_{k\in\mathcal{K}} s_k \tilde{\varphi}_k(t) e^{+jk\omega_{\rm sc}t} \right\} + n(t), \tag{3}$$

where $h_{\rm ch}(t)$ is the convolution of the channel impulse response (CIR) and the front-end band-selection filter $h_{\rm fef}(t)$, $\tilde{\varphi}_k(t)$ is the k-th sub-carrier pulse shape which is distorted by the channel $h_{\rm ch}(t)$, and $n(t)$ is filtered Gaussian noise.

The analog signal processing of the multichannel noncoherent autocorrelation receiver, c.f. Fig. 1, consists of a front end filter for frequency band selection and M AcR channels which perform the autocorrelation. The m-th AcR output is given as

$$y_m = \int_{\lambda=0}^{T_{\rm sym}} r(\lambda) \cdot r(\lambda - \tau_m) d\lambda \tag{4}$$

$$\approx \frac{1}{2} \sum_{k\in\mathcal{K}} s_k^2 \Re\left\{ \tilde{\Phi}_{kk}(\tau_m) e^{+j\omega_{\rm c}\tau_m} \right\} + \\ + \frac{1}{2} \sum_{k\in\mathcal{K}} \sum_{\substack{l\in\mathcal{K} \\ l\neq k}} s_k s_l \Re\left\{ \tilde{\Phi}_{kl}(\tau_m) e^{+j\omega_{\rm c}\tau_m} \right\} + \\ + \nu_m \tag{5}$$

$$\approx s_{\rm co}(\tau_m) + s_{\rm cross}(\tau_m) + \nu_m, \tag{6}$$

where τ_m is its delay time, $s_{\rm co}(\tau_m)$ is the signal co-terms, $s_{\rm cross}(\tau_m)$ is the the signal cross-terms, ν_m is the combination of all noise terms, and

$$\tilde{\Phi}_{kl}(\tau_m) = e^{+jl\omega_{\rm sc}\tau_m} \int_{\lambda=0}^{T_{\rm sym}} \tilde{\varphi}_k(\lambda) \tilde{\varphi}_l^*(\lambda - \tau_m) e^{+j(k-l)\omega_{\rm sc}\lambda} d\lambda \tag{7}$$

is the cross-correlation of the k-th and l-th basis function at given τ_m. Because the basis functions are assumed to be orthogonal for any delay τ_m, the cross-terms (where $l \neq k$) will vanish [4], [6]. For $l = k$ we get the autocorrelation of the k-th basis function at delay lag τ_m.

It can be seen from (7) that the autocorrelation terms ($l = k$) of the basis set map to baseband pulses plus an additional phase shift dependent on the sub-carrier frequency $l\omega_{\rm sc}$ and the AcR channel delay lag τ_m. A similar behavior can be seen for $l \neq k$, except that the baseband pulses are transformed to different frequencies $(k-l)\omega_{\rm sc}$. In Fig. 2, the co- and cross-terms, before integration, of a $K = 7$ sub-carrier UWB OFDM signaling scheme are depicted in the frequency domain.

Using vector notation we can rewrite (6) as

$$\mathbf{y} = \mathbf{H}\mathbf{s} + \mathbf{G}\,(\mathbf{s} \otimes \mathbf{s}) + \boldsymbol{\nu}, \tag{8}$$

where $\mathbf{H}$ is the MIMO channel matrix of the co-terms, $\mathbf{G}$ is the cross-terms interference matrix ($\otimes$ denotes the reduced Kronecker product), and $\boldsymbol{\nu}$ is the noise vector. This equation becomes $\mathbf{y} = \mathbf{H}\mathbf{s} + \boldsymbol{\nu}$ for orthogonal basis functions, given that the cross-terms vanish and therefore $\mathbf{G} = \mathbf{0}$.

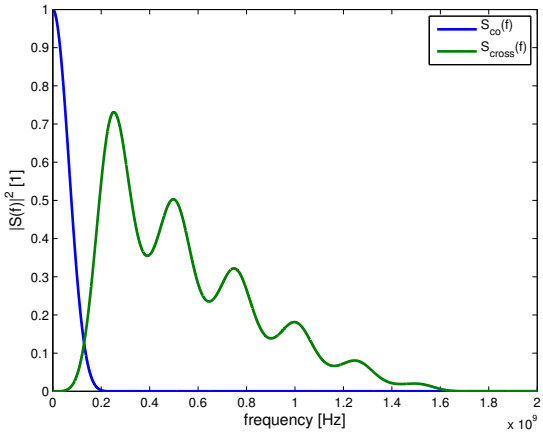

Fig. 2. Power spectrum density of the co- and cross-terms of an OFDM transmission scheme after the multiplication in an AcR channel for $K = 7$ sub-carrier UWB OFDM signaling scheme.

Assuming $M \geq K$ it is possible to reconstruct $\mathbf{s}$ using the Moore-Penrose pseudoinverse or a minimum-mean-square-error (MMSE) approach [6], [7], which is denoted by a transformation matrix $\mathbf{W}$. The decision variable vector $\mathbf{z}$ (c.f. Fig. 1) is therefore defined as

$$\mathbf{z} = \mathbf{W}\mathbf{y} \tag{9}$$

$$= \mathbf{W}\mathbf{H}\mathbf{s} + \mathbf{W}\mathbf{G}\,(\mathbf{s} \otimes \mathbf{s}) + \mathbf{W}\boldsymbol{\nu}. \tag{10}$$

III. Motivation

To minimize erroneous detection of $\mathbf{s}$, interference and noise have to be reduced. Because $\mathbf{s}$ is reconstructed by the linear transformation $\mathbf{W}$ of the AcR channel outputs $\mathbf{y}$, and M will be chosen only slightly greater than K for complexity reason, it is necessary to mitigate signal cross-terms and noise at the level of the AcR channel outputs y_m. These signal terms can be minimized by applying a low-pass filter (c.f Fig. 2).

In (7) it can be seen that the system has to perform an integration over the symbol period $T_{\rm sym}$. This operator can be described as a filter with the impulse response

$$h_T(t) = \sigma(t) - \sigma(t - T), \tag{11}$$

where T is the integration window, and $\sigma(t)$ is the unit step function. The frequency response of the filter is given as

$$H_T(j\omega) = T e^{-j\frac{T}{2}\omega} \mathrm{sinc}\left(\frac{T}{2\pi}\omega\right), \tag{12}$$

where $\mathrm{sinc}(x) = \frac{\sin(\pi x)}{\pi x}$ and ω is the angular frequency. Unfortunately, this ideal filter cannot be realized in real hardware. Therefore approximations of this ideal integration filter are needed.

Design goals for the filter approximation are a high output signal-to-noise ratio ($\mathrm{SNR}_{\mathbf{z}}$), which is defined as

$$\mathrm{SNR}_{\mathbf{z}} = \frac{\mathrm{E}\left\{\mathbf{s}^T\mathbf{H}^T\mathbf{W}^T\mathbf{W}\mathbf{H}\mathbf{s}\right\}}{\mathrm{E}\left\{\boldsymbol{\nu}^T\mathbf{W}^T\mathbf{W}\boldsymbol{\nu}\right\}}, \tag{13}$$

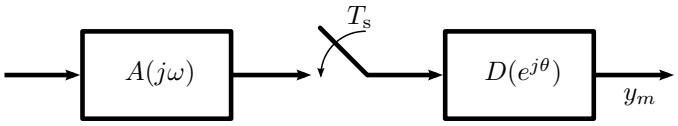

Fig. 3. Signal flow graph of the mixed-singal sliding window integrator.

and a high output signal-to-interference ratio ($\mathrm{SIR}_{\mathbf{z}}$), which is defined as (c.f. (6), (10))

$$\mathrm{SIR}_{\mathbf{z}} = \frac{\mathrm{E}\left\{\mathbf{s}^T\mathbf{H}^T\mathbf{W}^T\mathbf{W}\mathbf{H}\mathbf{s}\right\}}{\mathrm{E}\left\{(\mathbf{s}\otimes\mathbf{s})^T\mathbf{G}^T\mathbf{W}^T\mathbf{W}\mathbf{G}\,(\mathbf{s}\otimes\mathbf{s})\right\}}. \quad (14)$$

IV. Approximated Sliding Window Integrators

Approximation of the sliding window integrator (12) can be obtained using a low-pass Bessel filter and several notch-filters. The Bessel filter is used to get the magnitude frequency response and a constant group-delay up to an upper frequency, while the notch-filters are used for the zeros in the frequency response. For broadband signals this could lead to analog filters of very high order, due to the need of many notch filters. A mixed analog / digital implementation can relax this issue, as described below.

A. Approximation I

The impulse response (11) is rewritten as

$$h_T(t) = (\sigma(t) - \sigma(t - T_s)) * \sum_{k=0}^{N_T-1} \delta(t - kT_s), \quad (15)$$

where $T_s = \frac{T}{N_T}$, $N_T \in \mathbb{N}$. The sliding window integrator is split up into an integrator with a shorter window of length $\frac{T}{N_T}$ and a filter consisting of equally spaced Dirac impulses: a comb filter which can be described by a digital FIR filter easily, where T_s is the discrete-time sampling period. The comb filter has the discrete-time frequency response

$$D\left(e^{j\theta}\right) = \sum_{k=0}^{N_T-1} e^{-j\theta k}, \quad (16)$$

where θ is the normalized angular frequency, $\theta = \omega T_s$.

The new sliding window integrator $A(j\omega)$ is given by (12) but with reduced integration interval T_s. The frequency-spacing of the zeros increases when decreasing the integration interval, therefore the need of analog notch-filters *within the signal bandwidth* is relaxed. The digital filter introduces additional zeros at frequencies $\omega = k2\pi/(N_T T_s)$, $k \in \{\mathbb{Z} \mid (k \mod N_T) \neq 0\}$. In other words, the order of the analog filter is minimized by making the length of the sampling time T_s as small as possible. The accumulation of these partial integrations can be done by the digital comb filter without much effort.

The filter parameters (the upper frequency ($\mathrm{F_g}$) of constant group-delay of the Bessel filter and the quality factors ($\mathrm{Q_1}$, $\mathrm{Q_2}$) of the notch-filters) can be found numerically, applying

$$\boldsymbol{\theta}_\mathrm{I} = \arg\min_{\boldsymbol{\theta}} \frac{\int |H_T(f) - A(f,\boldsymbol{\theta})D(f)G(f,\boldsymbol{\theta})|^2\, df}{\int |H_T(f)|^2\, df}, \quad (17)$$

where $\boldsymbol{\theta}_\mathrm{I}$ is a parameter vector and $G(f,\boldsymbol{\theta}) = e^{j2\pi f\tau_\mathrm{g}}$ is a correction term for a constant group-delay difference between the ideal filter $H_T(f)$ and the approximation filter $A(f,\boldsymbol{\theta})D(f)$. The magnitude responses and the impulse responses of an example filter can be seen in Fig. 4.

B. Approximation II

Other filter approximations can be made too. A possibility is to reduce the combination of a low-pass filter and notch filters to a single Bessel type low-pass filter. Its upper frequency of constant group-delay $\mathrm{F_g}$ can be found applying

$$\mathrm{F_g} = \arg\min_{\mathrm{F_g}} \frac{\int ||H_T(f)| - |A(f,\mathrm{F_g})D(f)||^2\, df}{\int |H_T(f)|^2\, df}, \quad (18)$$

which is a simplification of (17) due to lower degree of freedom. The magnitude responses and the impulse responses of an example filter are illustrated in Fig. 4. Surprisingly this approximation can lead to a better performance than the ideal sliding window integrator.

V. Filter Analysis

To investigate the performance of the various sliding window integrator approximations $\mathrm{SNR}_{\mathbf{z}}$ and $\mathrm{SIR}_{\mathbf{z}}$ are considered, c.f Section III. The signaling scheme is a $K = 7$ sub-carrier UWB OFDM signal, where a truncated root-raised-cosine pulse was used with signal bandwidth and sub-carrier spacing of 250 MHz, and binary pulse position modulation (BPPM). This signaling scheme is used for the rest of the paper. The input signal $\frac{\mathcal{E}_\mathrm{b}}{N_0}$ (bit energy $\mathcal{E}_\mathrm{b}$ over noise spectral density N_0) was set to be 18 dB.

In Table I, the $\mathrm{SNR}_{\mathbf{z}}$ and $\mathrm{SIR}_{\mathbf{z}}$ values and filter parameters are listed for the two different approximation techniques, c.f. Section IV, as a function of the overall analog filter order. It can be seen, that the ideal sliding window integrator has the best $\mathrm{SIR}_{\mathbf{z}}$ performance, which is obvious when considering that the cross-terms should vanish completely for the ideal case. The $\mathrm{SIR}_{\mathbf{z}}$ of the second approximation method is in general higher than that of the first approximation with comparable filter order. This is due to the steeper frequency response of the second approximation filter that attenuates the high-frequency parts (i.e. the cross-terms) more heavily. The $\mathrm{SNR}_{\mathbf{z}}$ of the second approximation exceeds the $\mathrm{SNR}_{\mathbf{z}}$ of the ideal sliding window integration filter, due to the steeper magnitude response.

VI. System Simulations & Results

In Fig. 5 a comparison of the bit-error-rate (BER) of the aforementioned approximation methods is depicted. The simulated communication system and signals are described in Sections II and V. The resulting BER shows that both approximation methods are able to achieve similar performance compared with with an ideal sliding window integrator. Due to the better $\mathrm{SNR}_{\mathbf{z}}$, Approx. II shows the best BER results.

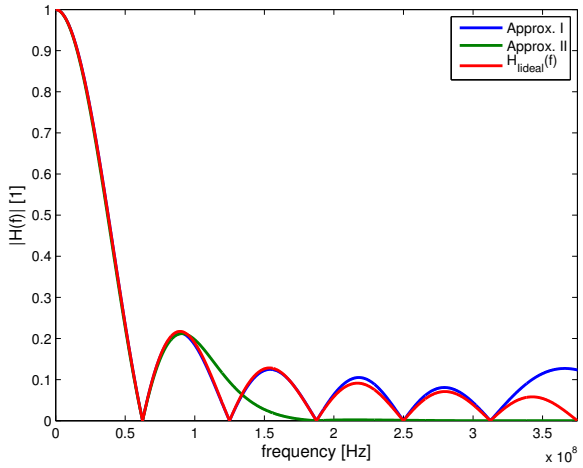

(a) Magnitude response

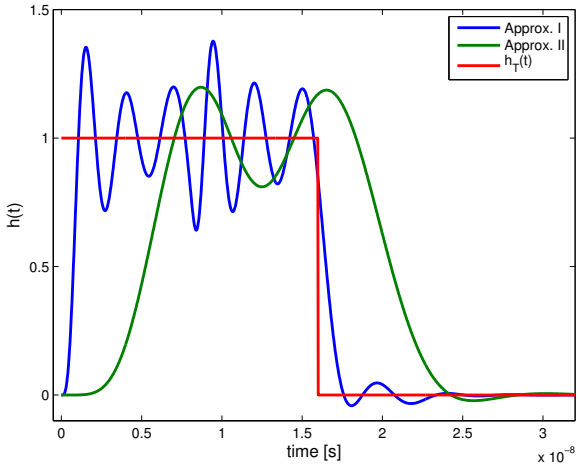

(b) Impulse response

Fig. 4. Magnitude response and impulse response of the Approx. I and Approx. II sliding window integrator.

TABLE I
ANALOG FILTER PARAMETERS (FILTER ORDER N, F_G, Q_1, AND Q_2) AND OUTPUT SNR (SNR_z) AND OUTPUT SIR (SIR_z) OF THE TWO FILTER APPROXIMATIONS. THE IDEAL INTEGRATOR HAS AN SNR_z OF 13.4 DB AND AN SIR_z OF 49.0 DB.

	Approx. I					Approx. II		
N	**F_g [MHz]**	**Q_1**	**Q_2**	**SNR_z [dB]**	**SIR_z [dB]**	**F_g [MHz]**	**SNR_z [dB]**	**SIR_z [dB]**
1						39.9	12.6	33.2
2						60.9	13.4	28.4
3						72.3	13.5	28.3
4						80.2	13.5	29.5
5	82.3	1.0	2.2	13.0	18.9	86.5	13.5	31.2
6	157.8	0.7	2.4	13.3	24.2	91.9	13.5	33.0
7	236.9	0.6	1.9	13.3	23.3	96.8	13.5	34.2
8	254.5	0.6	1.9	13.4	26.4	101.4	13.5	35.3
9	277.4	0.6	1.8	13.4	27.6	105.8	13.4	37.8
10	293.3	0.6	1.8	13.4	28.7	110.1	12.2	37.8

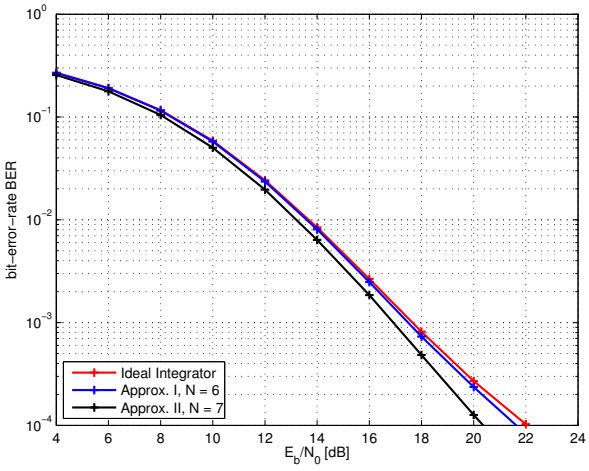

Fig. 5. BER for the given approximation setups in comparison to an ideal integrator.

VII. CONCLUSION

This work investigates approximation methods for ideal sliding window integrators. It has been shown that a simple mixed-signal system is able to perform a sliding window integration with low-complexity and rather high accuracy compared to the reference system with an ideal sliding window integrator. Additionally, it has been shown for the discused UWB OFDM scenario that the resulting mixed-signal implementation can exceed the performance of the reference system.

REFERENCES

[1] K. Witrisal, G. Leus, G. Janssen, M. Pausini, F. Troesch, T. Zasowski, and J. Romme, "Noncoherent ultra-wideband systems," *Signal Processing Magazine, IEEE*, vol. 26, no. 4, pp. 48 –66, 2009.

[2] T. Zasowski, F. Troesch, and A. Wittneben, "Partial channel state information and intersymbol interference in low complexity UWB PPM detection," Sep. 2006, pp. 369–374.

[3] S. Paquelet, L.-M. Aubert, and B. Uguen, "An impulse radio asynchronous transceiver for high data rates," in *Ultra Wideband Systems, 2004. Joint with Conference on Ultrawideband Systems and Technologies. Joint UWBST IWUWBS. 2004 International Workshop on*, may 2004, pp. 1 – 5.

[4] K. Witrisal, "Noncoherent autocorrelation detection of orthogonal multicarrier UWB signals," in *Ultra-Wideband, 2008. ICUWB 2008. IEEE International Conference on*, vol. 2, 2008, pp. 161 –164.

[5] L. Stoica, A. Rabbachin, H. Repo, T. Tiuraniemi, and I. Oppermann, "An ultrawideband system architecture for tag based wireless sensor networks," vol. 54, no. 5, pp. 1632–1645, Sep. 2005.

[6] P. Meissner and K. Witrisal, "Analysis of a noncoherent UWB receiver for multichannel signals," in *Vehicular Technology Conference, VTC2010-Spring*, IEEE, Ed., IEEE. Taipei: IEEE, May 2010, pp. 1 – 5. [Online]. Available: http://www.ieeevtc.org/vtc2010spring

[7] J. R. Barry, E. A. Lee, and D. G. Messerschmitt, *Digital Communication*. Springer Science+Business Media Inc., 2004.